ELSEVIER

Pattern Recognition Letters 21 (2000) 1209–1214

Pattern Recognition Letters

www.elsevier.nl/locate/patrec

Detection and classification of lobular and DCIS (small cell) microcalcifications in digital mammograms

Murk J. Bottema [a,b,*], John P. Slavotinek [c]

[a] *Department of Mathematics and Statistics Flinders University, P.O. Box 2100, Adelaide, SA 5001, Australia*
[b] *Cooperative Research Centre for Sensor Signal and Information Processing Warrendi Drive, Mawson Lakes, SA 4095, Australia*
[c] *Department of Medical Imaging, Flinders Medical Centre, Bedford Park, SA 5042, Australia*

Abstract

Microcalcifications are detected by fitting a model to every location in the mammogram. Model parameters yielding the best fit are used as features for detection and classification. The fraction of true positive (tp) detection is 60% with 1.23 false detections per cm^2. The rate of correct classification is 69%. © 2000 Elsevier Science B.V. All rights reserved.

Keywords: Microcalcifications; Breast cancer; Computer-assisted; Screening mammography; Detection

1. Introduction

Breast cancer is a major cause of death for women. Many countries recommend regular screening for women of certain age groups (usually 50–70 yr of age) and those belonging to other high risk groups. Although these programs are effective in reducing the mortality rate (Andersson, 1998; Thurfjell and Lindgren, 1994), 10–30% of cancers which could have been detected are missed (Bird et al., 1992; Duncan et al., 1998; Holland et al., 1982) (the wide range of these figures stems from the difficulty in defining what is meant by a missed cancer). In addition, a high percentage of patients called back at screening turn out not to have cancer (about 2/3 at BreastScreenSA which oversees screening in SA, Australia). In an effort to improve the accuracy of screening programs, many groups have investigated the possibility of using computers to assist radiologists in reading screening mammograms (Bottema and Slavotinek, 1999).

Clustered microcalcifications are one sign of cancer which has been the target of many studies on computer assisted screening. A linear filter, called the boxrim filter, was introduced in 1987 by a group at the University of Chicago (Chan et al., 1987) to form the basis of a detection scheme which was extended in subsequent papers (Chan et al., 1988; Ema et al., 1995; Nishikawa et al., 1993). Similar approaches using Gaussian filters (Zheng et al., 1995) and splines (Maitournam et al., 1998) instead of the boxrim filter have been described as well as methods using wavelets (Qian et al., 1995; Strickland and Hahn, 1996; Zhang et al., 1998), fractals (Lefebvre and Benali, 1995; Li et al., 1997), and neural networks (Chan et al., 1995; Zhang et al., 1996; Zheng et al., 1996).

The detection of calcification is important, but since a large percentage of normal mammograms

* Corresponding author. Fax: +61-8-8201-2904.
E-mail address: murkb@ist.flinders.edu.au (M.J. Bottema).

PII: S0167-8655(00)00083-0

also show some calcification, detection by itself is only of limited value. Classifying calcification as being associated with a benign or malignant process requires extracting features of diagnostic importance from the image. Examples of features reported in the literature for this purpose include the number of calcifications in the cluster, mean area of calcifications, variation in computed density, variation in volume, shape irregularity, circularity, statistical properties of the intensity surface, properties of co-occurrence matrices, statistical properties of the distribution of calcifications within the cluster, and fractal dimension of the surrounding tissue (Dhawan et al., 1998; Jiang et al., 1996; Thiele et al., 1996; Wu et al., 1995). Many of these features (but not all) are ones that radiologists use in assessing mammograms.

Although several studies report high detection and classification rates (Jiang et al., 1996; Wu et al., 1995; Zhang et al., 1998), there are some prevailing problems.

1. Most calcifications are easy to detect both visually and via a computer algorithm. If a detection scheme finds 90% of all clusters there is a danger that it has found roughly the same 90% that the radiologist discovers without assistance. Using a random collection of mammograms showing calcification for training and testing algorithms probably biases the routine toward finding clusters which offer little additional diagnostic value.
2. Detection algorithms reported in the literature target all classes of calcifications at once, despite the fact that there are huge varieties in shape, size, and contrast.
3. Although the emphasis has rightly been focused on detecting clusters of calcifications, once a cluster is detected, classification depends on measuring features from a diverse collection of individual calcifications within the cluster. So while a few prominent calcifications might suffice to detect the cluster, improved classification may well depend on detecting and analyzing subtle examples.
4. Many of the features listed in the previous paragraph for use in classification are not meaningful if the calcification is represented by only a few pixels.

Our group seeks to mitigate these problems by developing different detecting schemes for different classes of microcalcifications. In this way, detection is (hopefully) improved by being more focused and classification is boosted by information supplied by the various schemes. In this paper, attention is restricted to the detection of small, more or less spherical calcifications. This is done by constructing a model for such calcifications based on the projection of a ball of constant density. By varying the radius and density of the model, a best fit is found. The values of radius and density which provide the best fit are used to decide if the candidate is a true calcification or not.

2. Methods and materials

2.1. Calcification model

The measured intensity of an X-ray beam may be modeled as

$$I(x) = I_0 \mathrm{e}^{-\int_L f(z)\,\mathrm{d}z}, \tag{1}$$

where I_0 is the source intensity, $f(z)$ the X-ray attenuation at a point z in space, x the projection of z onto the image plane, and L is the path of the X-ray beam from the source to the detector (film). Scattering is ignored and X-ray beams are assumed to be parallel. Our model consists of a ball of constant X-ray attenuation, μ, embedded in tissue. We assume that the contribution to the image intensity surface of the tissue surrounding the ball is well approximated by a plane at the scale of the ball (0.4 mm or less). Thus locally, the measured intensity is

$$I(x) = I_0 \mathrm{e}^{-\mu s(x) - (a + bx)}, \tag{2}$$

where a is a constant, b a constant vector, and s is the length of the segment formed by the intersection of L and the ball. If the ball has radius R and is centered above the origin,

$$s(x) = \begin{cases} 2\sqrt{R^2 - \|x\|^2}, & \text{if } R^2 - \|x\|^2 \geqslant 0, \\ 0, & \text{otherwise.} \end{cases} \tag{3}$$

The connection between density and X-ray attenuation, the film response, and the characteristics of

the digitizer are all approximated by linear processes so that the shape of the model is not altered. After suitable transformation of the raw image data, the model for the calcification in the mammogram is given by

$$h(x) = a + bx + \lambda\sqrt{R^2 - \|x\|^2}, \tag{4}$$

where a, b, λ and R are to be determined. The value of λ is only related to the density of the calcification, but it will be referred to as density for simplicity.

2.2. Data

Film mammograms were obtained from the archives of BreastScreenSA in Adelaide, SA, Australia. Cases showing cancer were included only if verified by pathology and normals were included only if no cancer was found after 3 yr. Films were digitized at 50 μ resolution and 12 bit depth using a Lumisys Lumiscan 150 laser digitizer.

The images were reviewed and electronically annotated by a radiologist experienced in mammography (JPS) to indicate the location of clusters of microcalcifications. In six of the images, the location of 113 individual calcifications were marked.

2.3. Detection of microcalcifications

The detection algorithm comprises preliminary detection of candidate calcifications, model fitting, and parameter estimation, and finally deciding if the candidate is a true calcification or not.

2.3.1. Preliminary detection

The boxrim filter of Chan et al. (1987) was used to identify the candidate of microcalcifications. A threshold was chosen just high enough so that connected sets in the resulting binary image formed mainly isolated convex sets. Large (more than 80 pixel) connected sets were discarded as were sets of irregular shape. The density of connected components in the resulting binary image is roughly 150 sets per cm^2 so the locations of true calcifications are very likely to be represented. For each such set, the location of the maximum value was adopted as the center of a candidate calcification. These steps are displayed in Fig. 1.

2.3.2. Model fitting and feature extraction

For each candidate location in the image, estimates of a, b, λ, and R were determined by minimizing

$$E(a, b_1, b_2, \lambda, R) = \sum_{(i,j)\in\Omega} \phi^2(i,j), \tag{5}$$

where

$$\phi(i,j) = g(i,j) - [a + b_1 i + b_2 j + \lambda s(i,j)], \tag{6}$$

$g(i,j)$ is the image intensity value at (i,j), Ω a discrete approximation of the disk of radius $\sqrt{2}R$ centered at the candidate location, and s is as in

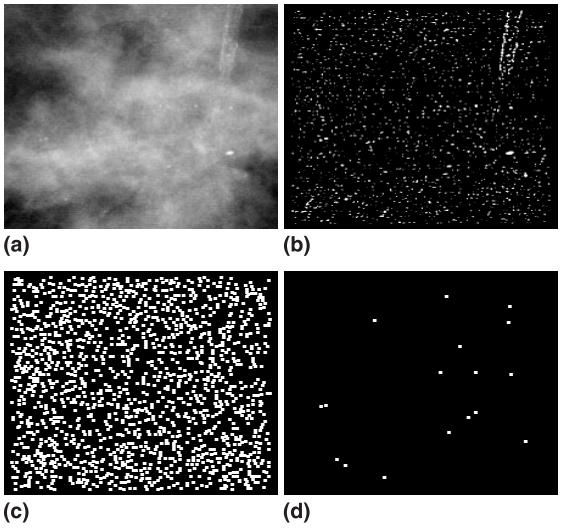

Fig. 1. (a) A region showing a cluster of calcifications of lobular type. (b) The image after applying the boxrim filter and thresholding. Calcified artery walls are clearly seen in the upper right corner. (c) Each connected component in (b) has been replaced by a single pixel located at the maximum intensity value within the component. For display purposes, each such pixel is represented by a 3×3 patch. The large obvious calcification is not included and the irregular patches in the upper right corner of (b) have also been correctly rejected. (d) The locations judged by the algorithm to correspond to true calcifications. This particular image provided the poorest detection rate and highest fp rate of those tested but is interesting for its diversity.

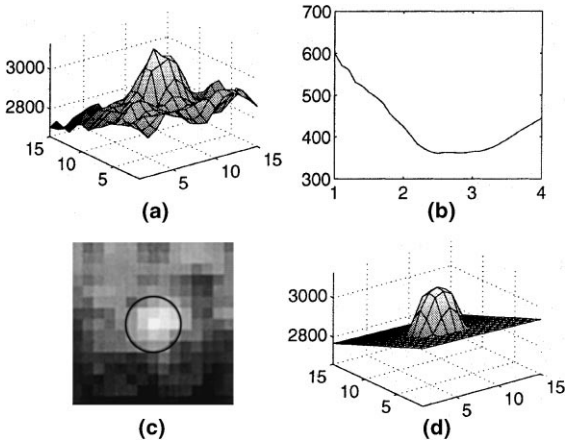

Fig. 2. (a) A surface plot of a calcification. Note that the background exhibits local fluctuation plus a gradual change in intensity. (b) A plot of the error, E, as a function of the radius of the model. The smallest error in this example was found with $R = 2.5$. (c) A plan view of the calcification with a circle of $R = 2.5$ centered on the local peak intensity value. The gradual background change is also apparent in this representation. (d) The best fit model for this example.

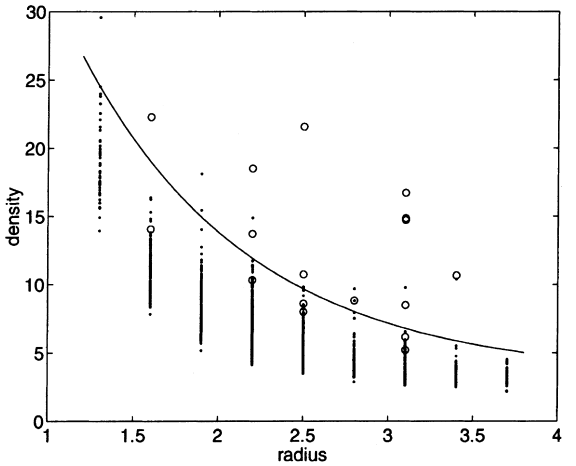

Fig. 3. True calcifications are marked "o" and other candidates are marked "•". The solid line is the curve in Eq. (7).

Eq. (3). For fixed R, ϕ is linear in a, b_1, b_2, and λ, so simple regression was used to find optimal values for these parameters.

The minimum of E over all parameters was found by repeating this process for different values of R (Fig. 2). In the experiments reported here, the values of R used were $1.0, 1.3, 1.6, \ldots, 4.0$.

2.3.3. Detection criteria

Detection was based solely on the radius, R, and the density parameter, λ, of the best fitting model. The radius and density were estimated for approximately 3000 candidate calcifications of which 34 were true calcifications as indicated by the radiologist. A decision curve to separate true and false candidates was constructed as described in the next paragraph based on all true and false examples with estimated radius less than 4 pixels (Fig. 3).

For each radius R, the histogram of measured densities of false candidates showed an abrupt upper limit $\lambda_0(R)$ beyond which very few (<0.2%) measurements were recorded. The decision curve was generated by finding the best fitting exponential function through the points $(R_i, \lambda_0(R_i))$. The resulting curve is given by

$$d(R) = 4.2 + 77.8298\,\mathrm{e}^{-0.9985R}. \tag{7}$$

(The choice of fitting an exponential curve is heuristic. Since λ is a surrogate for density, the observed trend may be a consequence of dimensionality, but further investigation is required.)

Two additional criteria were imposed. The first was aimed at eliminating artifacts due to film flaws. These appear as very bright intensity values restricted to a cluster of about 4 pixels or less. After examining the location of known artifacts of this type, an upper limit of density was set at 40. The second criterion stemmed from the fact that best fit models with minimum or maximum radius are not reliable. Because only finitely many radii were allowed, true calcifications with large radii end up with best fits at maximum value of the radius, regardless of the true radius. Also, locations which do not resemble the model well for any set of parameters are likely to find the best fit by matching the single pixel local maximum which provided their status as candidate calcification during preprocessing.

In summary, a candidate was judged to be a calcification if

$$d(R) < \lambda < 40 \quad \text{and} \quad 1.5 < R < 4.0. \tag{8}$$

2.4. Classification of calcifications

The detection algorithm assigned 109 locations as being the site of a calcification within a cluster (calcifications detected in isolation are routinely dismissed as not being of diagnostic interest). Of these, 60 were from clusters of ductal carcinoma in situ (DCIS) (small cell) and 49 were from clusters of lobular calcifications. DCIS clusters are associated with cancers and lobular microcalcifications are an example of a benign type. All locations found by the detection algorithm, whether marked as true calcifications by the radiologist or not, were classified as being lobular or DCIS (small cell) based solely on the goodness of fit value, E. The motivation for using this criterion is that lobular calcifications tend to be round and smooth while DCIS (small cell) tend to be generally spherical but with irregular surfaces.

3. Results

Table 1 summarizes the detection rates for the algorithm described here and for a previous version (Bottema and Slavotinek, 1998). For training and testing images, the percentage of true positive (tp) detections is given and the false positive (fp) rate is given in terms of the number of false positive detections per cm^2. The algorithm was also applied to a number of "normal" images, meaning cases where no indications of cancer were found at screening and no cancer developed within 3 yr.

The higher rate of true detection in the test set compared with the training set may be due to insufficient randomization in dividing the available cases into test and training sets.

Of the 60 locations found by the detection algorithm within known clusters of DCIS (small cell) microcalcifications, 72% were correctly identified as DCIS (small cell) by classification based only on the goodness of fit parameter, E. This classification was per individual calcification and did not consider parameter values of neighboring calcifications. Of the 49 lobular microcalcifications, 65% were identified correctly. The overall rate of correct classification for the two types of calcification together was 69%.

4. Discussion

For reasons stated in the introduction, attention was restricted to clusters of calcifications which are difficult to detect. In particular, only calcifications of radius less than 0.2 mm were considered. In comparing the performance with our previous work, a moderate reduction in the detection rate was well compensated for by a substantial reduction in the fp detection rate.

The performance of the detecting algorithm is difficult to assess independently of the performance of a full scheme for computer assisted screening mammography. Table 1 reports the percent of true detections, but this is based on the radiologists judgement. The disease state of the tissue associated with the cluster can be ascertained by histopathology, but the location of individual calcifications cannot be verified. This problem is exacerbated by the fact that only subtle calcifications are of primary interest. In some instances, locations recorded as fps, were later identified by the radiologist as possible or probable calcification.

The ultimate goal is to decide if there are clusters of microcalcifications associated with cancer. From this point of view, the question of whether a certain location represents no calcification or a benign calcification is moot. Accordingly, the purpose of the algorithm for initial detection is not necessarily to detect just microcalcifications, but to detect points in the image which serve as a basis

Table 1
Detection rates

Method	Train (% tp)	Train (fp)	Test (% tp)	Test (fp)	Normal (fp)
Current	59	0.79	60	1.23	0.56
Previous	63	1.68	77	3.21	1.82

for correct classification of the image as showing signs of a malignant cluster or not. The results suggest that locations other than those identified by an experienced radiologist as representing microcalcifications can contribute to identification of cancer. This suggestion is currently being investigated.

References

Andersson, I., 1998. Breast cancer screening results. In: Karssemeijer, N., Thijssen, M., Hendriks, J., van Erning, L. (Eds.), Fourth International Workshop on Digital Mammography.

Bird, R.E., Wallace, T.W., Yankaskas, B.C., 1992. Analysis of cancers missed at screening mammography. Radiology 184 (3), 613–617.

Bottema, M.J., Slavotinek, J.P., 1998. Detection of subtle microcalcification in digital mammograms. In: Karssemeijer, N., Thijssen, M., Hendriks, J., van Erning, L. (Eds.), Fourth International Workshop on Digital Mammography.

Bottema, M.J., Slavotinek, J.P., 1999. Computer aided screening mammography. In: Pham, B., Braun, M., Maeder, A.J., Eckert, M. (Eds.), New Approaches in Medical Image Analysis, SPIE. Vol. 3747, pp. 177–190.

Chan, H.-P., Doi, K., Galhorta, S., Vyborny, C.J., MacMahon, H., Jokich, P.M., 1987. Image feature analysis and computer-aided diagnosis in digital radiography. I. Automated detection of microcalcifications in mammography. Med. Phys. 14 (4), 538–548.

Chan, H.-P., Doi, K., Vyborny, C.J., Lam, K.-L., Schmidt, R.A., 1988. Computer-aided detection of microcalcifications in mammograms methodology and preliminary clinical study. Invest. Radiol. 23 (9), 664–671.

Chan, H.-P., Lo, S.-C.B., Sahiner, B., Lam, K.L., Helvie, M.A., 1995. Computer-aided detection of mammographic microcalcifications: Pattern recognition with an artificial neural network. Med. Phys. 22 (10), 1555–1567.

Dhawan, A.P., Chitre, Y., Kaiser-Bonasso, C., Moskowitz, M., 1998. Analysis of mammographic microcalcifications using gray-level image structure features. IEEE Trans. Med. Imaging 15 (3), 246–259.

Duncan, K.A., Needham, G., Deans, H.E., 1998. Incident round cancers: what lessons can we learn?. Clin. Radiol. 53, 29–32.

Ema, T., Doi, K., Nishikawa, R.M., Jiang, Y., Papaioannou, J., 1995. Image feature analysis and computer-aided diagnosis in mammography: reduction of false-positive clustered microcalcifications using local edge-gradient analysis. Med. Phys. 22 (2), 161–169.

Holland, R., Mravunac, M., Hendriks, J.H.C.L., Bekker, B.V., 1982. So-called interval cancer of the breast: pathologic and radiologic analysis of sixty-four cases. Cancer 49 (12), 2527–2533.

Jiang, Y., Nishikawa, R.M., Wolverton, D.E., Metz, C.E., Giger, M.L., Schmidt, R.A., Vyborny, C.J., Doi, K., 1996. Malignant and benign clustered microcalcifications: automated feature analysis and classification. Radiology 198 (3), 671–678.

Lefebvre, F., Benali, H., 1995. A fractal approach to the segmentation of microcalcifications in digital mammograms. Med. Phys. 22 (4), 381–390.

Li, H., Liu, K.J.R., Lo, S.-C.B., 1997. Fractal modeling and segmentation for the enhancement of microcalcifications in digital mammograms. IEEE Trans. Med. Imaging 16 (6), 785–798.

Maitournam, A., Graffigne, C., Strauss, A., 1998. Modeling of digital mammograms using bicubic spline functions and additive noise. In: Karssemeijer, N., Thijssen, M., Hendriks, J., van Erning, L. (Eds.), Fourth International Workshop on Digital Mammography.

Nishikawa, R.M., Giger, M.L., Doi, K., Vyborny, C.J., Schmidt, R.A., 1993. Computer-aided detection of clustered microcalcifications: an improved method for grouping detected signals. Med. Phys. 20 (6), 1661–1666.

Qian, W., Kallergi, M., Clarke, L.P., Li, H.-D., Venugopal, P., Song, D., Clark, R.A., 1995. Tree structured wavelet transform segmentation of microcalcifications in digital mammography. Med. Phys. 22 (8), 1247–1254.

Strickland, R.N., Hahn, H.I., 1996. Wavelet transforms for detecting microcalcifications in mammograms. IEEE Trans. Med. Imaging 15 (2), 218–229.

Thiele, D.L., Kimme-Smith, C., Johnson, T.D., McCombs, M., Bassett, L.W., 1996. Using tissue texture surrounding calcification clusters to predict benign vs malignant outcomes. Med. Phys. 23 (4), 549–555.

Thurfjell, E.L., Lindgren, J.A.A., 1994. Population-based mammography screening in Swedish clinical practice: prevalence and incidence screening in uppsala county. Radiology 193, 351–357.

Wu, Y.C., Freedman, M.T., Hesegawa, A., Zuurbier, R.A., Lo, S.-C.B., Mun, S.K., 1995. Classification of microcalcifications in radiographs of pathologic specimens for the diagnosis of breast cancer. Acad. Radiol. 2 (3), 199–204.

Zhang, W., Doi, K., Giger, M.L., Nishikawa, R.M., Schmidt, R.A., 1996. An improved shift-invariant artificial neural network for computerized detection of clustered microcalcifications in digital mammograms. Med. Phys. 23 (4), 595–601.

Zhang, W., Yoshida, H., Nishikawa, R.M., Doi, K., 1998. Optimally weighted wavelet transform based on supervised training for detection of microcalcifications in digital mammograms. Med. Phys. 25 (6), 949–956.

Zheng, B., Chang, Y.-H., Staiger, M., Good, W., Gur, D., 1995. Computer-aided detection of clustered microcalcifications in digitized mammograms. Acad. Radiol. 2 (8), 655–662.

Zheng, B., Qian, W., Clarke, L.P., 1996. Digital mammography: mixed feature neural network with spectral entropy decision for detection of microcalcifications. IEEE Trans. Med. Imaging 15 (5), 589–597.